

Effect of the alidade thermal behavior on the pointing accuracy of a large radio telescope

Shan-Xiang Wei^{1,2,3}, De-Qing Kong^{1,3*} and Qi-Ming Wang^{2,3**}

¹ Key Laboratory of Lunar and Deep Space Exploration, National Astronomical Observatories, Chinese Academy of Sciences, Beijing 100101, China; weishanxiang@bao.ac.cn; kdq@bao.ac.cn; qmwang@bao.ac.cn

² Key Laboratory of FAST, National Astronomical Observatories, Chinese Academy of Sciences, Beijing 100101, China

³ University of Chinese Academy of Sciences, Beijing 100049, China

Received 2020 December 15; accepted 2021 January 12

Abstract The alidade's non-uniform temperature field of a large radio telescope is very obvious under solar radiation. Estimating a radio telescope's pointing errors, caused by the alidade deformation under solar radiation, is significant to improve the telescope's pointing accuracy. To study the effect of the alidade thermal behavior on the pointing accuracy of a large radio telescope, a temperature experiment is first carried out in a 70-m radio telescope on a sunny day. According to the measured results, the temperature distribution rule of the alidade is summarized initially. In addition, the alidade's temperature field is calculated by finite element thermal analysis. The simulated results are proved to be in good agreement with the experimental results. Finally, the alidade deformation under solar radiation is computed by finite element thermal-structure coupling analysis. The telescope's pointing errors caused by alidade deformation are estimated via the alidade's node displacements. The final results show that the effect of alidade thermal behavior on the telescope's elevation pointing errors $\Delta\varepsilon_2 + \Delta\varepsilon_r$ is much more than the effect on the telescope's cross-elevation pointing errors $\Delta\varepsilon_1$. The maximum of $\Delta\varepsilon_2 + \Delta\varepsilon_r$ is more than $45''$, while the maximum of $\Delta\varepsilon_1$ is less than $6''$. This study can provide valuable references for improving the pointing accuracy of large radio telescopes.

Key words: telescopes — finite element analysis — thermal behavior — pointing accuracy

1 INTRODUCTION

Large radio telescopes are widely employed in astronomical research and deep space exploration. A typical large-scale and fully-steerable radio telescope, Wuqing 70-m radio telescope, is shown in Figure 1.

The telescope structures consist of five parts: the subreflector and quadripod, the main reflector and backup structure, the elevation cradle, the alidade structure, and the azimuth rail. As the foundation of a radio telescope, the alidade can move around the vertical azimuth axis on the azimuth rail. The elevation cradle and the above structures, connected with the alidade by two elevation bearings, can rotate around the horizontal elevation axis as a whole (Baars & Kärcher 2018). Generally, good pointing accuracy is expected for a radio telescope to receive radio waves from the universe accurately. Affected

by gravity, solar radiation, and wind disturbance, a large radio telescope's structural deformation is inevitable. Without proper compensation or restraint for these effects, a radio telescope's pointing accuracy can hardly meet the observation requirements. The gravity-induced deformation of a radio telescope is repeatable, and the corresponding pointing error can be estimated by the classic pointing model (Kong et al. 2014). However, the thermal deformation and the wind-induced deformation of a radio telescope are time-varying, and the corresponding pointing errors are also dynamic (Ranka et al. 2016; He et al. 2020). The dynamic pointing errors would seriously affect the regular operation of a radio telescope on sunny days with strong winds. Therefore, estimating a telescope's dynamic pointing errors, caused by solar radiation and wind disturbance, is very significant for improving the telescope's pointing accuracy.

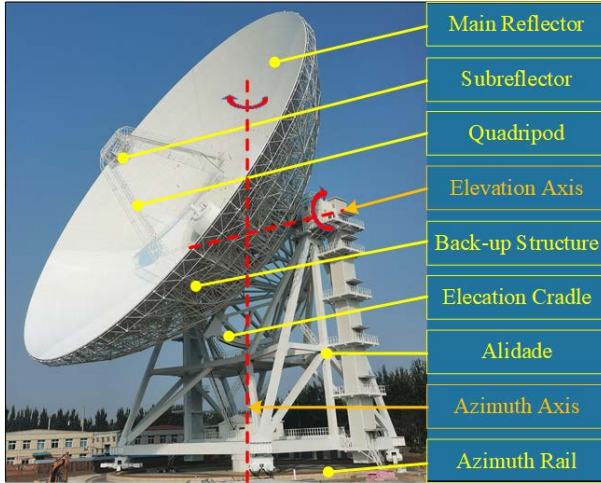
The thermal design and thermal behavior of some radio telescopes were discussed internationally before

* Corresponding author

** Corresponding author

Table 1 List of Experimental Instruments

Instrument	Specification	Tested Range	Precision	Function
Thermometer	PT100	−100 to 400 °C	0.1 °C	Testing temperature
Temperature analyzer	ZJ1064	−100 to 400 °C	0.1 °C	Collecting temperature data
Solar power meter	SM206	0.1 to 2000 W m ^{−2}	5%	Testing solar radiation
Anemometer	AS816	0.3 to 30 m s ^{−1}	5%	Testing wind speed

**Fig. 1** 70 m radio telescope.

2010. The corresponding research results have been collected in Albert Greve's book (Greve & Bremer 2010), including the IRAM 30-m telescope (Greve et al. 2005), the Medicina 32-m telescope (Pisanu et al. 2010), the ALMA prototype antennas (Greve & Mangum 2008), and so on. Besides, the effects of the rail and the thermal gradient on pointing errors of Sardinia 64-m radio telescope were also studied by experimental measurement and astronomical observation in 2014 (Pisanu et al. 2014). In China, related studies also have been carried out in several radio telescopes in recent years. The temperature distribution of FAST 500-m radio telescope under solar radiation was studied by National Astronomical Observatories (Song et al. 2011; Song & Wang 2016). The electromechanical coupling analysis of a 7.3-m radio telescope under solar radiation was conducted by Xidian University via finite element (FE) calculations (Li et al. 2012; Wang et al. 2017). The alidade temperature behavior of Tianma 65-m radio telescope was analyzed by Shanghai Astronomical Observatory through the measurements of inclinometers and thermometers (Fu et al. 2016; Fu et al. 2019). According to a series of temperature experiments, the axis-angle errors of Miyun 50-m radio telescope under solar radiation were discussed by National Astronomical Observatories (Kong et al. 2019). Combining experiment and FE method to study radio telescope's thermal behavior proved to be effective in IRAM 30-m telescope (Greve et al. 2005), but has been less applied in China's large radio telescopes so far.

The Wuqing 70-m radio telescope is the largest fully steerable radio telescope in China, the thermal behavior of which should never be ignored. In this paper, the 70-m radio telescope's alidade (hereinafter referred to as the alidade) is considered the research object. Combining the experiment and FE analysis, the non-uniform temperature field of the alidade under solar radiation is analyzed. The telescope's pointing errors caused by the alidade deformation are estimated. In Section 2, the temperature experiment is described, and the experimental results are discussed. In Section 3, the temperature distributions of the alidade are analyzed through FE thermal analysis. The simulated results are verified by the experimental results. In Section 4, the thermal deformations of the alidade are computed through FE thermal-structure coupling analysis. The pointing errors caused by the alidade deformation are estimated via extracting the alidade's node displacements. In Section 5, the conclusion is completed.

2 EXPERIMENTAL STUDY OF THE ALIDADE'S SOLAR TEMPERATURE FIELD

A temperature experiment of the alidade was conducted on 2020 October 3. The day was clear, and the average wind speed was less than 1 m s^{−1}. The position at the elevation angle of 90° and the azimuth angle of 180° was set as the radio telescope's locked position during the experiment.

2.1 Experiment Preparation

The purpose of this experiment is to obtain the temperature distribution rule of the alidade and verify the FE thermal-analysis results about the solar temperature field of the alidade. It is impossible to install temperature sensors at all nodes of the alidade's FE thermal-analysis model. Actually, only 20 temperature sensors are installed at some special locations of the alidade to study the alidade's temperature distribution rule under solar radiation, as shown in Figure 2. The corresponding experimental instruments are listed in Table 1.

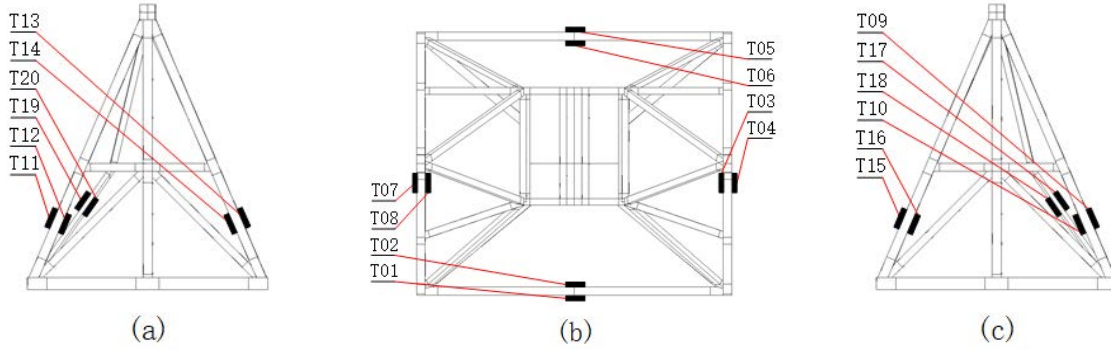
2.2 Experimental Results

The measured temperatures of the 20 test points on the alidade on 2020 October 3 are shown in Figure 3.

The experimental results show that solar radiation and shadow coverage have significant effects on the alidade's

Table 2 Material Properties of Alidade

Material	Density kg m^{-3}	Specific Heat $\text{J kg}^{-1} \text{K}^{-1}$	Thermal Conductivity $\text{W m}^{-1} \text{K}^{-1}$	Thermal Expansion 10^{-6}K^{-1}
Steel	7850	465	49.8	11.59

**Fig. 2** Distribution of thermometers on the alidade: (a)right view, (b)top view, (c)left view.

temperature field. According to Figure 3, the temperature distribution rule of the alidade on 2020 October 3 can be summarized as follows.

(1) The temperatures of the test points facing the south, including T01, T09, T11, T17, and T19, but except T06, increased quickly from 7:00 and reached the maximum of 28.9°C, 28.7°C, 28.9°C, 30.7°C, and 29.6°C respectively at 14:30, due to solar radiation without self-shadow coverage. In contrast, the temperatures of the test point T06 facing the south were always closed to the values of the test point T05 facing the north, owing to the shadow coverage of the main reflector and elevation platform.

(2) The temperatures of the test points facing the east, including T03 and T08, increased quickly from 7:00 to 10:00 owing to solar radiation. The temperatures were then slowly closed to the ambient air temperature due to the self-shadow coverage.

(3) The temperatures of the test points facing the west, including T04 and T07, were less than the ambient air temperature from 7:00 to 12:00, due to the self-shadow coverage and long-wave radiation. After 12:00, the values increased quickly and reached the maximum at 16:00 owing to solar radiation.

(4) The non-uniform temperature field of the alidade under solar radiation was evident, and the maximum temperature difference was up to 10.4°C in the daytime.

3 THEORETICAL STUDY OF THE ALIDADE'S SOLAR TEMPERATURE FIELD

Heat transfer occurs through heat conduction, convection and radiation. The basic theories of the above three types of heat exchange are perfect in thermodynamics and will not be covered here. The heat transfer process of alidade

will be affected by some complex factors. These factors will be discussed here, including material properties, the temperatures for sky and ground, the coefficients for convection and radiation, and the shadow coverage of the main reflector and elevation platform, and so on (Greve & Bremer 2010).

3.1 FE Model and Boundary Conditions

The FE model of the alidade is shown in Figure 4. The element type of the alidade's thermal-analysis model is shell131, and the corresponding structural element is shell181. The material properties of the alidade are shown in Table 1.

The boundary conditions of the alidade's FE thermal analysis are consistent with the experimental conditions on 2020 October 3. Some environmental parameters have been measured in the experiment, including ambient air temperatures, wind speeds, and solar radiation intensity. These measured values will be applied in the alidade's FE thermal analysis here.

The sky temperature T_s can be expressed as (Greve & Bremer 2010)

$$T_s(t) = 0.0553T_a^{1.5}(t), \quad (1)$$

and the ground temperature T_g can be expressed as (Greve & Bremer 2010)

$$T_g(t) = T_a(t) + \Delta T_g(t), \quad (2)$$

where T_a is the temperature of ambient air, ΔT_g is a temperature offset and it can be approximately expressed as $10 \sin[(t - 8)\pi/12]$ here (Qian et al. 2016), and t is the local time. In addition, considering the white paint surface layer of the alidade, the solar absorption rate of

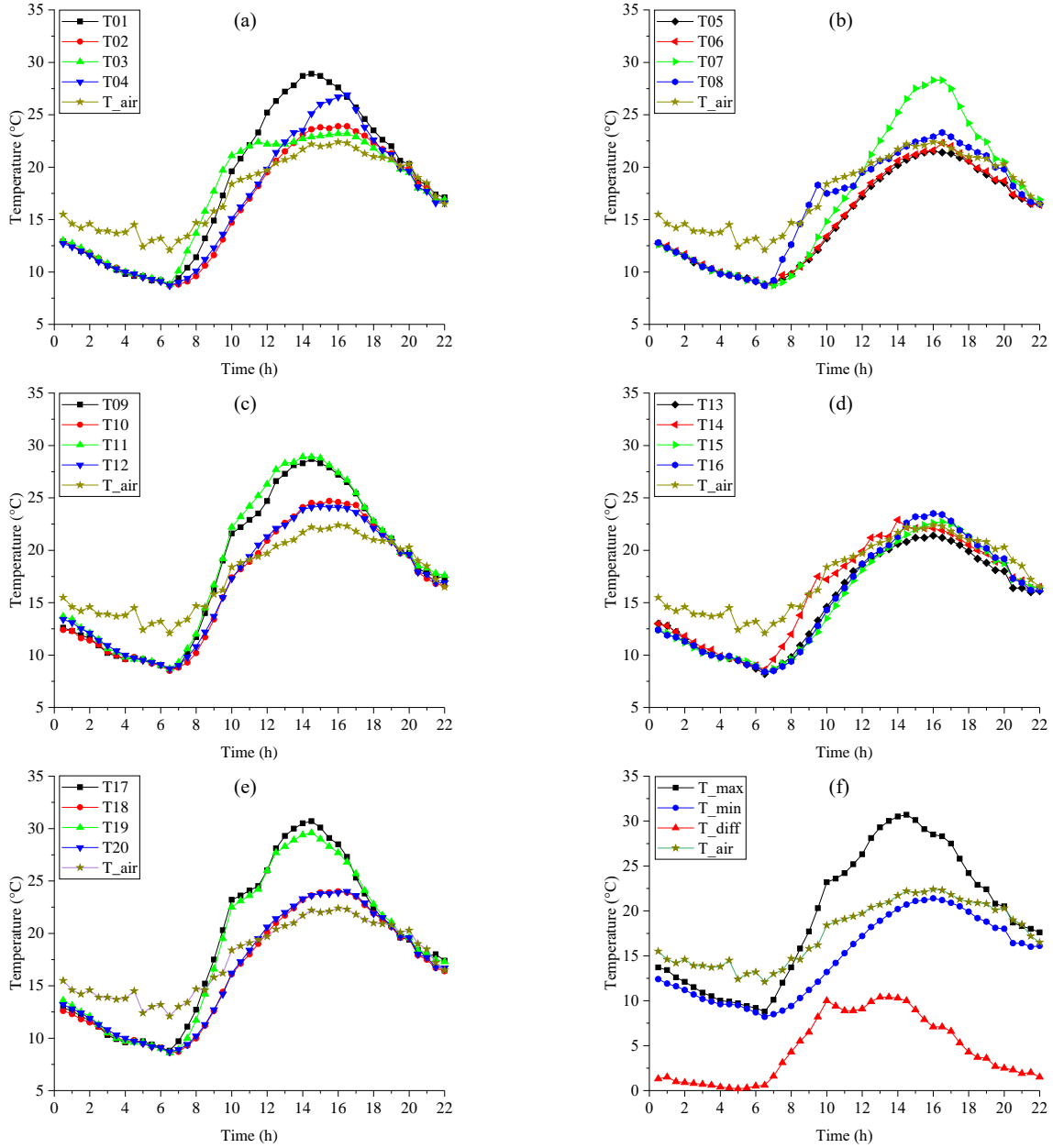


Fig. 3 Measured temperatures at the 20 test points of alidade: (a) T01~T04, (b) T05~T08, (c) T09~T12, (d) T13~T16, (e) T17~T20, (f) maximum temperature(T_{max}), minimum temperature(T_{min}) and maximum temperature difference(T_{diff}) among the 20 test points.

the structure is set as 0.25. The surface reflectance of the 70-m radio telescope site in a rough lawn is 0.26.

3.2 Convection Coefficient and Radiation Coefficient

The air convection can be treated as the surface loads to act on the alidade's meshed elements directly. The convective heat transfer coefficient h_c can be given as (Greve & Bremer 2010)

$$h_c = 0.664R_e^{1/2}P_r^{1/3}k/L, \quad (3)$$

where the Reynolds Number $R_e = vL\rho(z)/\mu$, the Prandtl Number $P_r = \mu/\rho(z)\alpha$, the air thermal diffusivity $\alpha = k/\rho(z)\ell$, v is the wind speed, $\rho(z)$ is the air density related with altitude, μ is the air absolute viscosity, ℓ is the air heat capacity at constant pressure, and k is the air thermal conductivity.

The radiations, including solar radiation, sky radiation, and ground radiation, can be treated as the equivalent heat generation rate to act on the alidade's meshed elements. For a tilted plane exposed to solar radiation on the alidade, the angle coefficient $\cos\theta_t$ for solar radiation can be

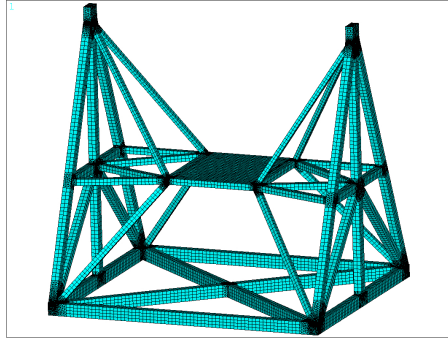


Fig. 4 FE thermal-analysis model of alidade.

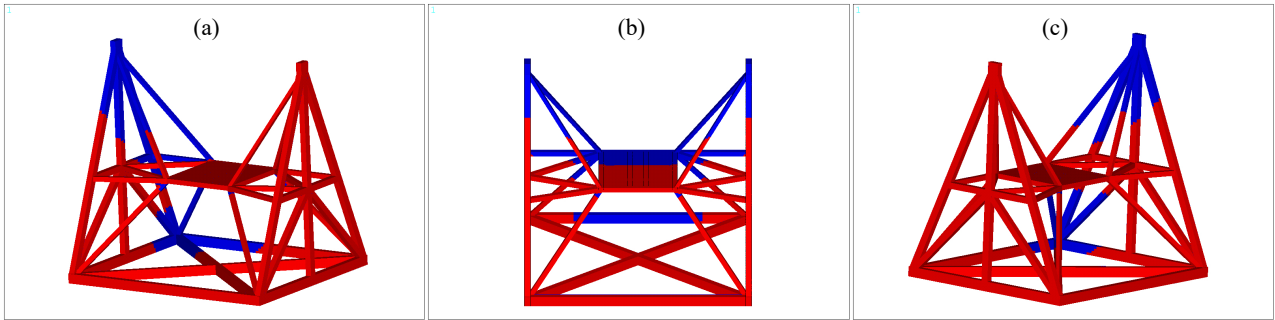


Fig. 5 Shadow distributions of the alidade under solar radiation: (a)10:00, (b)12:00, (c)15:00.

calculated as (Greve & Bremer 2010)

$$\cos \theta_t = \cos \theta_z \cos \beta + \sin \theta_z \cos \psi \sin \beta, \quad (4)$$

where θ_t is the incident angle of the solar beam on the tilted plane, θ_z is the zenith angle of the Sun, β is the tilt angle of the tilted plane, ψ is the azimuth difference between the tilted plane and the solar beam. The angle coefficient φ_s for sky radiation can be expressed as (Chen et al. 2016)

$$\varphi_s = (1 + \cos \beta)/2 \quad (5)$$

and the angle coefficient φ_g for ground radiation can be expressed as (Chen et al. 2016)

$$\varphi_g = (1 - \cos \beta)/2, \quad (6)$$

where β is same as Equation (4).

3.3 Shadow Distribution

The shadow distribution of a radio telescope is related to the working condition of the telescope and the Sun's position. The shadow distribution of the alidade is mainly affected by the shadow coverage of both the main reflector and the elevation platform under solar radiation. The alidade's shadow distribution can be computed by the ray casting algorithm. Figure 5 shows the alidade's shadow distributions at 10:00, 12:00, and 15:00 on 2020 October 3. The red parts represent the planes exposed to solar radiation, and the blue regions represent the shadow-covered planes.

3.4 Simulated Results and Verification

The alidade's temperature distributions can be calculated by FE transient thermal analysis. Figure 6 shows the calculated temperature contours of the alidade at different times on 2020 October 3. The simulated results show that the alidade's non-uniform temperature field under solar radiation is very obvious, and there is a time lag between the temperature distributions and the shadow distributions.

Several representative test points on the alidade, including T01, T03, T05, T07, T11, and T19, are chosen to verify the above thermal-analysis results. T01, T03, T05, and T07 in the alidade's bottom face the south, the east, the north, and the west, respectively. T11 and T19 in the alidade's middle face the south. The comparison of both experimental temperature and simulated temperature for the selected test points are shown in Figure 7. The simulated average error rate is shown in Figure 8. The results show that the temperature trends of both experiment and simulation are in good agreement, and the maximum error rate is less than 0.2.

4 EFFECT OF THE ALIDADE DEFORMATION UNDER SOLAR RADIATION ON POINTING ERROR

The alidade structure and the elevation cradle of the 70-m radio telescope are connected by two elevation bearings. As shown in Figure 9 (left), the two elevation bearings

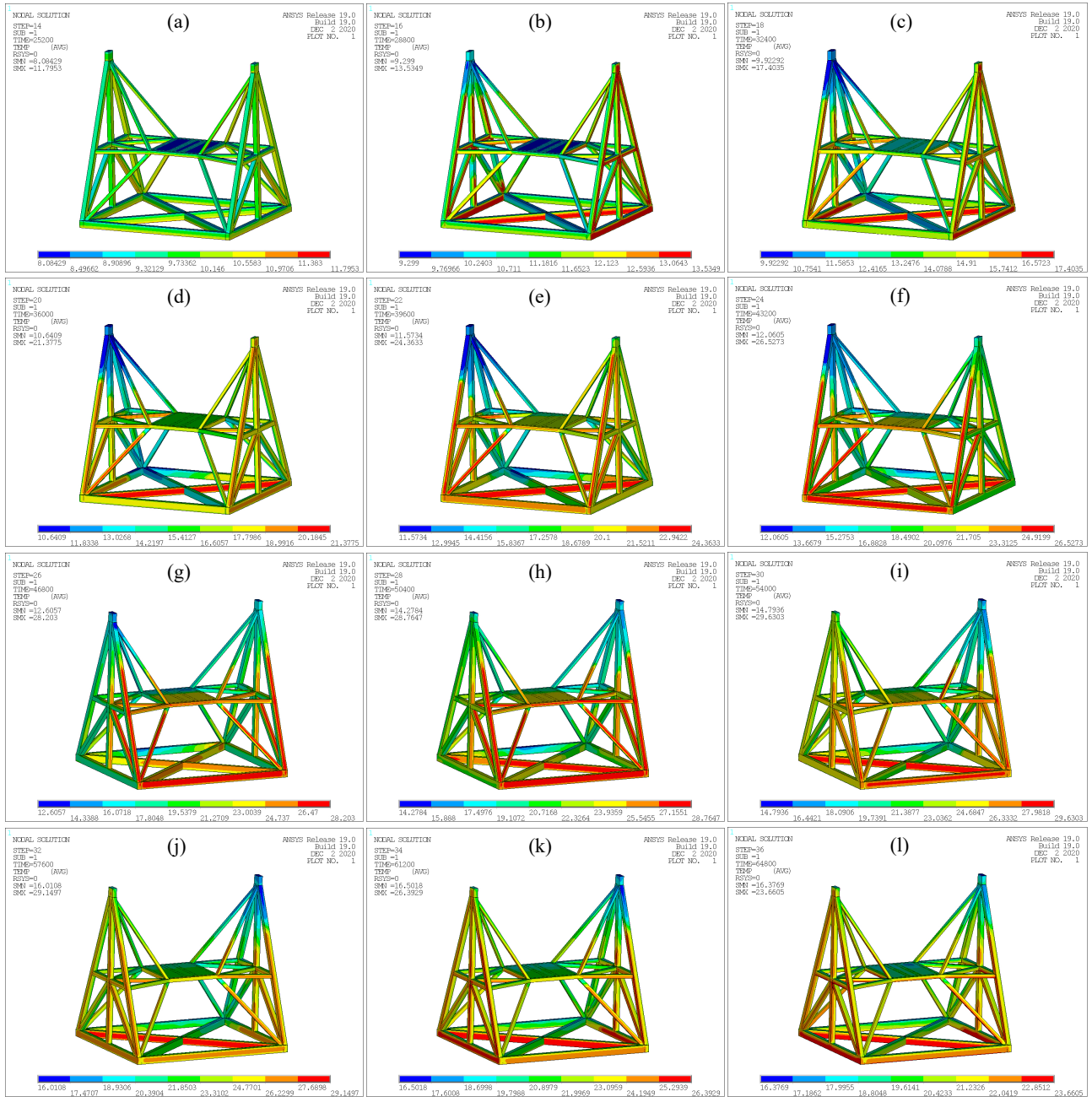


Fig. 6 Temperature contours of the alidade at different times: (a) 7:00, (b) 8:00, (c) 9:00, (d) 10:00, (e) 11:00, (f) 12:00, (g) 13:00, (h) 14:00, (i) 15:00, (j) 16:00, (k) 17:00, (l) 18:00.

are installed at the A_1 -tower top point M and the A_2 -tower top point N. The elevation driver is installed at point P. The two azimuth drivers are installed at point D and point E. The alidade deformation under solar radiation will affect the pointing errors of the telescope. As shown in Figure 9 (right), the alidade’s axis-angle errors, including the tilt angle along the horizontal elevation axis, the tilt angle along the vertical azimuth axis, and the rotation angle around the elevation axis, can directly affect the radio telescope’s pointing accuracy. The alidade thermal deformation will be analyzed, and the corresponding

pointing errors caused by the alidade deformation will be discussed here.

4.1 Alidade Deformation under Solar Radiation

Before the structural analysis, the boundary conditions of the alidade’s FE structural model should be set. First, all freedoms for node D and node E are restricted. The movements along the Z-axis for node F and node G are also not allowed. The rotation of node H around the Z-axis is the only freedom. Then, the alidade’s thermal-analysis

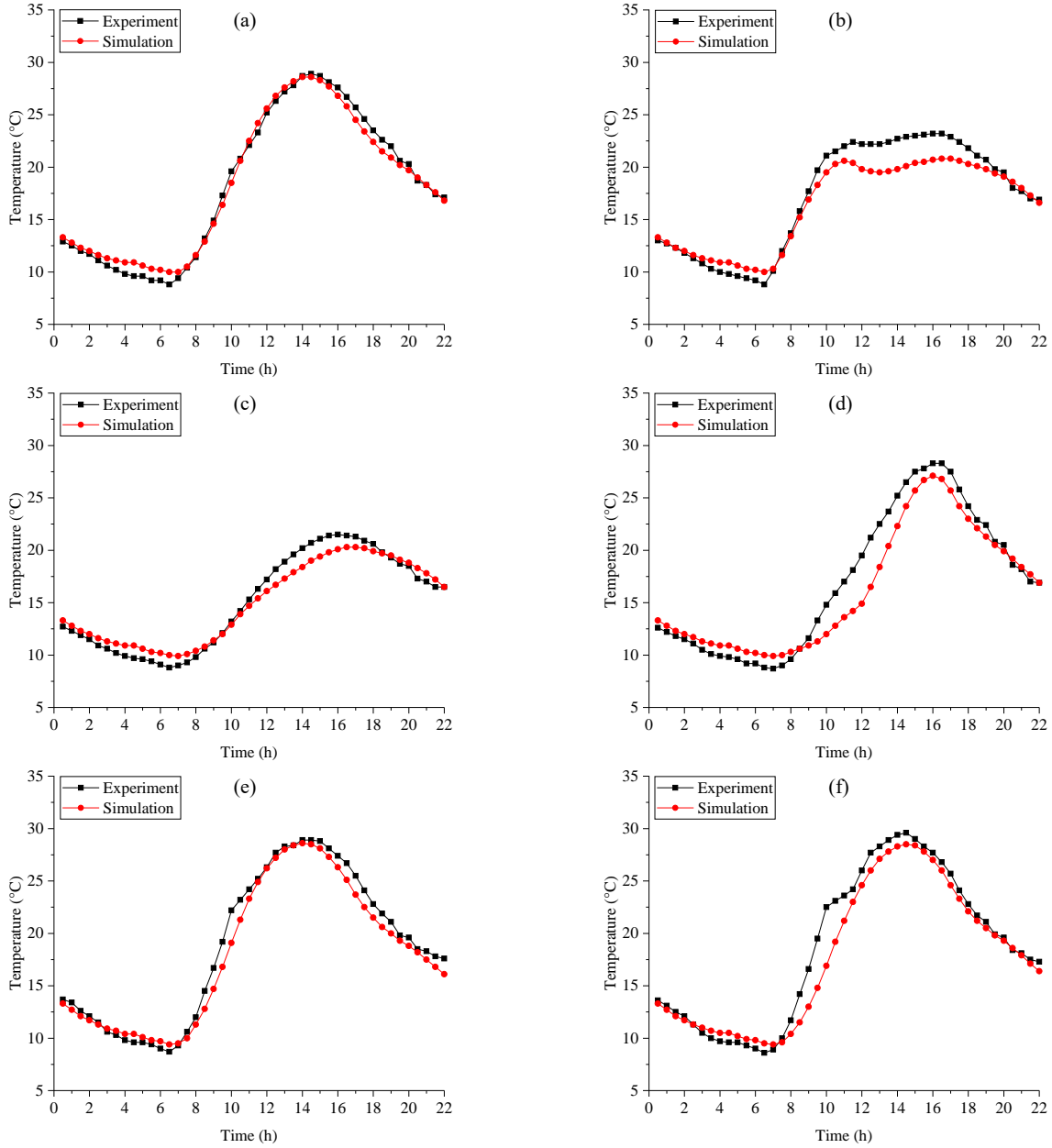


Fig. 7 Comparison of both experimental temperature and simulated temperature for several special test points: (a) T01, (b) T03, (c) T05, (d) T07, (e) T11, (f) T19.

results are loaded onto the FE structural model. In addition, the gravity of both the elevation cradle and the above structures is treated as the uniform pressures to act on the elevation bearing boxes. The gravity acceleration is set as 9.8 m s^{-2} . Finally, the alidade deformation is computed by FE analysis. The displacement contours of the alidade along the Y -axis are shown in Figure 10.

4.2 Pointing Errors Caused by the Alidade Deformation under Solar Radiation

The alidade's towers of A_1 and A_2 with different temperatures under solar radiation would deform to

different degrees. As shown in Figure 9 (right), the difference ΔL between the deformed displacement of A_1 -tower top point M and the deformed displacement of A_2 -tower top point N in a vertical plane would cause the cross-elevation pointing error $\Delta\varepsilon_1$ of the radio telescope. $\Delta\varepsilon_1$ cannot be detected directly by encoders, but can be estimated as (Greve & Bremer 2010)

$$\Delta\varepsilon_1 = \Delta L/l, \quad (7)$$

where $\Delta L = \text{sign}(z_N - z_M) \sqrt{(y_N - y_M)^2 + (z_N - z_M)^2}$. y_M and z_M are the displacements of A_1 -tower top point M along the Y -axis and the Z -axis, respectively. y_N and

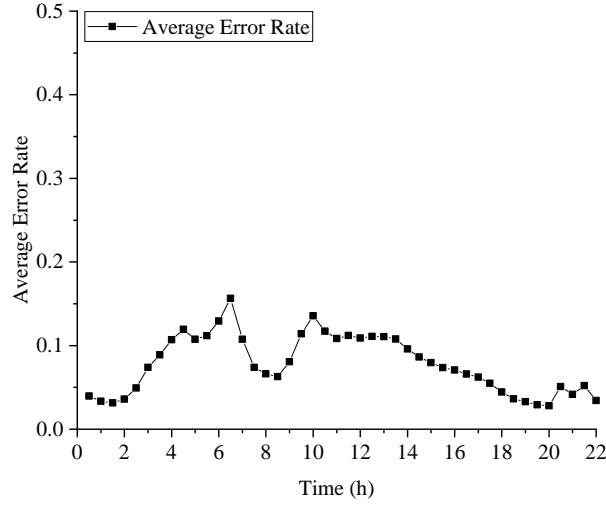


Fig. 8 Average error rate of simulated temperatures at all test points.

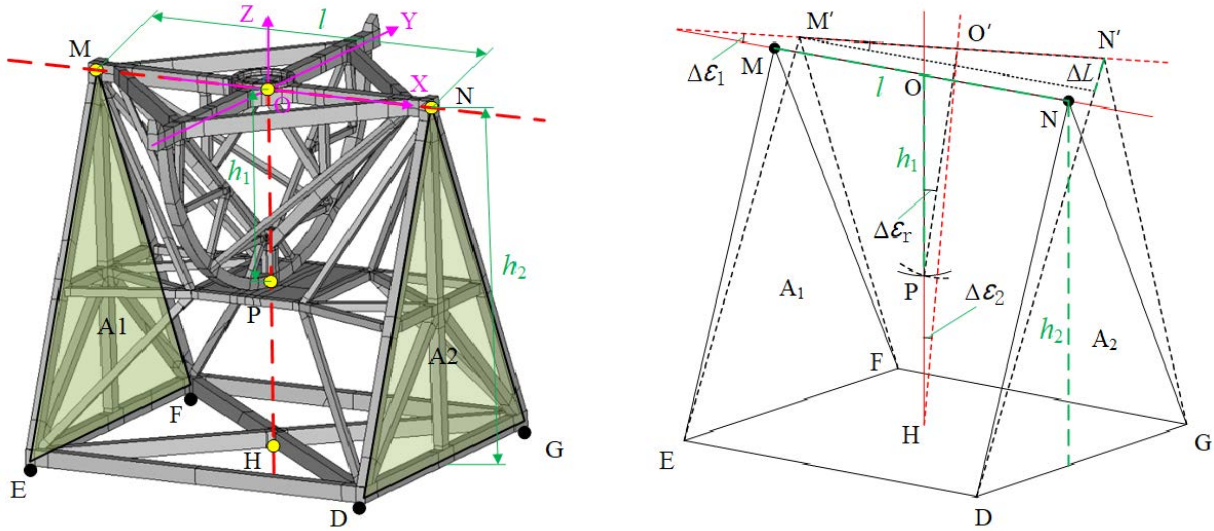


Fig. 9 Alidade 3D structure (left) and alidade deformation analysis (right).

z_N are the displacements of A_2 -tower top point N along the Y -axis and the Z -axis, respectively. In addition, l is the width of the alidade. Specially, the cross-elevation pointing error $\Delta\varepsilon_1$ can be divided into two components, including the horizontal cross-elevation pointing error $\Delta\varepsilon_a$ and the vertical cross-elevation pointing error $\Delta\varepsilon_v$. $\Delta\varepsilon_a$ can be expressed as $(y_M - y_N)/l$ and calibrated by changing the azimuth angle of the radio telescope. $\Delta\varepsilon_v$ can be given as $(z_N - z_M)/l$ but cannot be calibrated directly.

Similarly, the differential thermal expansion between the front and the rear of the alidade under solar radiation would result in the radio telescope's elevation pointing error. The elevation pointing error caused by the alidade deformation consists of the tilted elevation pointing error $\Delta\varepsilon_2$ and the rotated elevation pointing error $\Delta\varepsilon_r$.

Generally, $\Delta\varepsilon_r$ can be detected by encoders and calibrated by the closed-loop control, but $\Delta\varepsilon_2$ is hard to detect and calibrate. $\Delta\varepsilon_2$ and $\Delta\varepsilon_r$ can be respectively expressed as (Greve & Bremer 2010)

$$\Delta\varepsilon_2 = (y_N + y_M)/2h_2, \quad (8)$$

and

$$\Delta\varepsilon_r = [(y_N + y_M)/2 - y_P]/h_1, \quad (9)$$

where y_P is the Y -axis displacement of point P . h_1 is the distance between the horizontal elevation axis and the elevation driver. h_2 is the height of the horizontal elevation axis from the azimuth rail.

The pointing errors of the 70-m radio telescope caused by the alidade thermal deformation on 2020 October 3 are shown in Figure 11, where T_{aa} is the average temperature difference between the A_1 -tower and the A_2 -tower. T_{fr} is

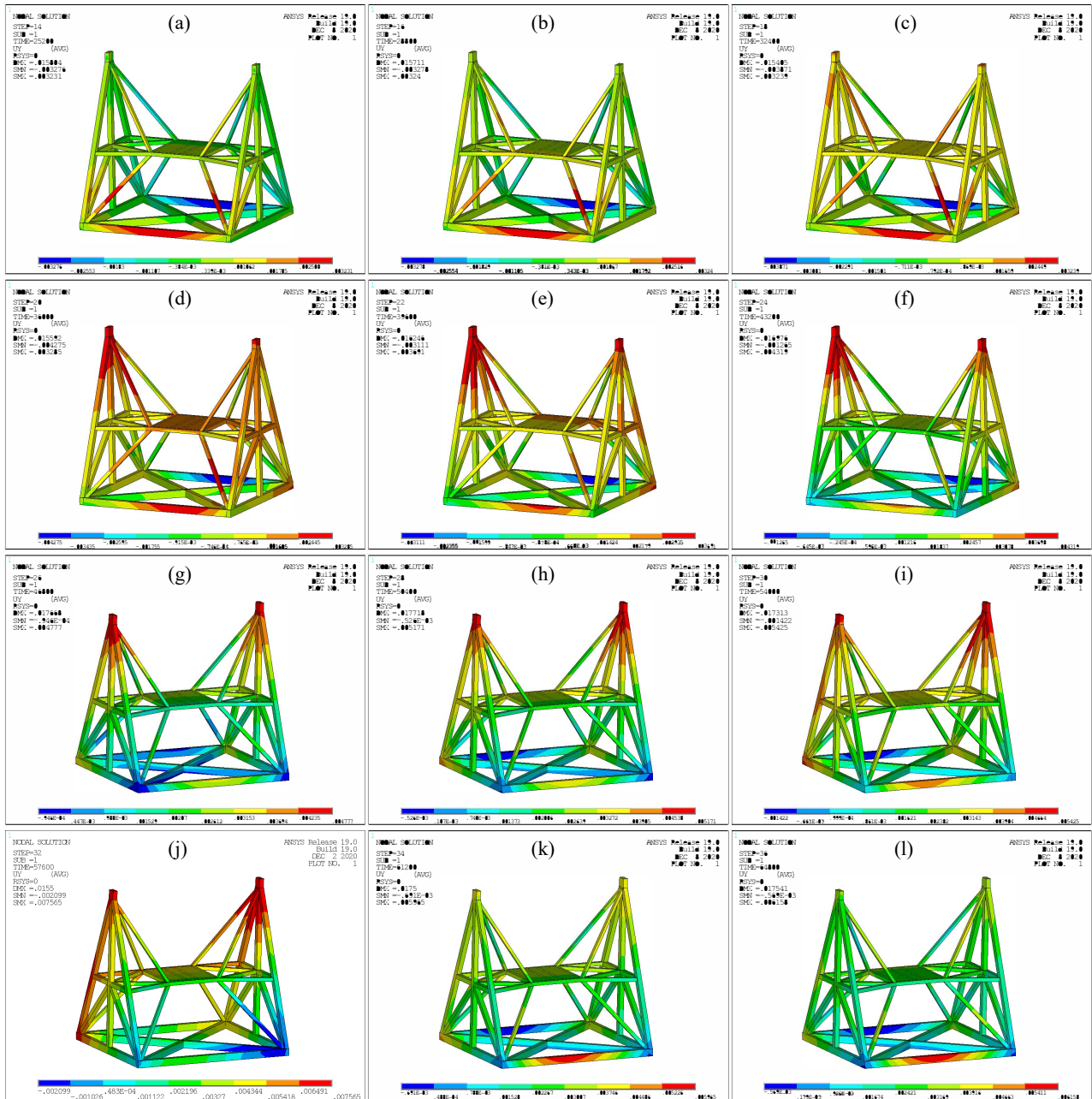


Fig. 10 Displacement contours of the alidade along the Y-axis at different times: (a) 7:00, (b) 8:00, (c) 9:00, (d) 10:00, (e) 11:00, (f) 12:00, (g) 13:00, (h) 14:00, (i) 15:00, (j) 16:00, (k) 17:00, (l) 18:00.

the average temperature difference between the front and the rear of the alidade. The results show that the trends of both $\Delta\varepsilon_1$ and T_{aa} are in good agreement. In addition, $\Delta\varepsilon_2 + \Delta\varepsilon_r$ is closely related to T_{tr} . Furthermore, the effect of the alidade thermal behavior on the elevation pointing error $\Delta\varepsilon_2 + \Delta\varepsilon_r$ is much more than the effect on the cross-elevation pointing error $\Delta\varepsilon_1$.

5 CONCLUSIONS

The Wuqing 70-m radio telescope is taken as the research object in this paper. First, the temperature experiments

of alidade are conducted on a sunny day, and the temperature distribution rule is summarized. Second, the non-uniform temperature field of alidade is simulated by FE analysis and verified by experiment. Finally, the alidade deformation under solar radiation is calculated. The pointing errors of the telescope caused by the alidade deformation are estimated. According to the research results, the conclusion can be drawn as follows.

- (1) The alidade’s non-uniform temperature field under solar radiation is pronounced. The maximum measured

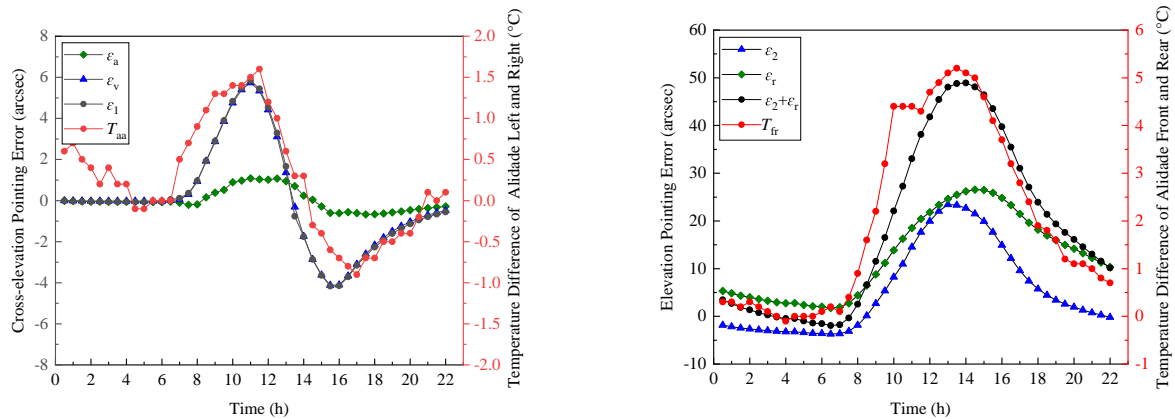


Fig. 11 Cross-elevation pointing error(*left*) and elevation pointing error(*right*) of the 70-m radio telescope.

temperature difference reached 10.4°C in the experiment on 2020 October 3.

(2) The alidade's temperature distribution can be computed well by FE analysis. The simulated average error rates are less than 0.15 most of the time.

(3) The telescope's cross-elevation pointing error $\Delta\varepsilon_1$, caused by the alidade deformation, is related to the temperature gradient between the left and the right of the alidade. The telescope's elevation pointing error $\Delta\varepsilon_2 + \Delta\varepsilon_r$, caused by the alidade deformation, is related to the temperature gradient between the front and the rear of the alidade.

(4) $\Delta\varepsilon_2 + \Delta\varepsilon_r$ is much more than $\Delta\varepsilon_1$ under solar radiation. On 2020 October 3, the maximum of $\Delta\varepsilon_2 + \Delta\varepsilon_r$ was more than $45''$, while the maximum of $\Delta\varepsilon_1$ was less than $6''$.

Acknowledgements This work was funded by the Astronomical Joint Fund of National Natural Science Foundation of China and Chinese Academy of Sciences (U1831114) and the National Natural Science Foundation of China (11673040 and 11803053).

References

- Baars, J. W. M., & Kärcher, H. J. 2018, Radio Telescope Reflectors, 447 (Springer International Publishing AG)
- Chen, D. S., Qian, H. L., Wang, H. J., et al. 2016, Applied Thermal Engineering, 111, 1130
- Fu, L., Ling, Q. B., Geng, X. G., et al. 2016, in Society of Photo-Optical Instrumentation Engineers (SPIE) Conference Series, 9912, Advances in Optical and Mechanical Technologies for Telescopes and Instrumentation II, eds. R. Navarro, & J. H. Burge, 99124J
- Fu, L., Wang, J., Jiang, Y., et al. 2019, Experimental Astronomy, 48, 49
- Greve, A., & Bremer, M. 2010, Thermal Design and Thermal Behaviour of Radio Telescopes and their Enclosures, 364 (Springer)
- Greve, A., Bremer, M., Penalver, J., Raffin, P., & Morris, D. 2005, IEEE Transactions on Antennas and Propagation, 53, 851
- Greve, A., & Mangum, J. 2008, IEEE Antennas and Propagation Magazine, 50, 66
- He, F.-L., Xu, Q., Wang, N., & Zhu, C.-H. 2020, RAA (Research in Astronomy and Astrophysics), 20, 199
- Kong, D. Q., Jiang, Z. Y., Zhang, H. B., & Wu, Y. X. 2019, Scientia Sinica Technologica (in Chinese), 49, 1331
- Kong, D.-Q., Wang, S.-G., Wang, J.-Q., Wang, M., & Zhang, H.-B. 2014, RAA (Research in Astronomy and Astrophysics), 14, 733
- Li, P., Duan, B. Y., Wang, W., & Zheng, F. 2012, IEEE Antennas and Propagation Magazine, 54, 40
- Pisanu, T., Buffa, F., Morsiani, M., Pernechele, C., & Poppi, S. 2010, in Society of Photo-Optical Instrumentation Engineers (SPIE) Conference Series, 7739, Modern Technologies in Space- and Ground-based Telescopes and Instrumentation, eds. E. Atad-Ettdgui, & D. Lemke, 773935
- Pisanu, T., Buffa, F., Poppi, S., et al. 2014, in Society of Photo-Optical Instrumentation Engineers (SPIE) Conference Series, 9145, Ground-based and Airborne Telescopes V, eds. L. M. Stepp, R. Gilmozzi, & H. J. Hall, 91454R
- Qian, H. L., Chen, D. S., Fan, F., Liu, Y., & Shen, S. Z. 2016, International Journal of Steel Structures, 16, 383
- Ranka, T., Garcia-Sanz, M., Symmes, A., Ford, J. M., & Weadon, T. 2016, Journal of Astronomical Telescopes, Instruments, and Systems, 2, 014001
- Song, L. Q., & Wang, Q. M. 2016, in Society of Photo-Optical Instrumentation Engineers (SPIE) Conference Series, 9682, 8th International Symposium on Advanced Optical Manufacturing and Testing Technologies: Large Mirrors and Telescopes, eds. M. K. Cho, & B. Fan, 968204
- Song, L. Q., Wang, Q. M., & Guo, Y. W. 2011, Optics and Precision Engineering (in Chinese), 19, 951
- Wang, C. S., Yuan, S., Liu, X., et al. 2017, Radio Science, 52, 1253